Aggregation of fibrils and plaques in amyloid molecular systems

Mario Nicodemi,[1,2] Antonio de Candia,[2,3] and Antonio Coniglio[2,3]
[1]*Department of Physics and Complexity Science Centre, University of Warwick, Coventry, United Kingdom*
[2]*INFN, Napoli, Italy*
[3]*Dipartimento di Scienze Fisiche, Università di Napoli "Federico II," Napoli, Italy*
(Received 21 July 2009; published 12 October 2009)

Amyloidlike proteins form highly organized aggregates, such as fibrils and plaques, preceded by the assembly of a wide range of unstructured oligomers and protofibrils. Despite their importance in a number of human neurodegenerative diseases, a comprehensive understanding of their kinetics and thermodynamics is still missing. We investigate, by computer simulations, a realistic model of amyloid molecules interacting via the experimentally determined Derjaguin-Landau-Verwey-Overbeek potential and derive its phase diagram. We show that fibrils and plaques, along with their precursors, correspond to different equilibrium and metastable thermodynamics phases and discuss the dynamical mechanisms leading to the nucleation and self-assembly of large scale structures.

DOI: 10.1103/PhysRevE.80.041914 PACS number(s): 87.14.em, 87.15.A−, 64.60.Cn

I. INTRODUCTION

Amyloidlike proteins are known to form highly organized aggregates, such as fibrils and plaques, which associate with a variety of human conditions, including type II diabetes and neurodegenerative diseases [1] (e.g., Alzheimer, Parkinson, etc.). Advances have recently been made to elucidate the structures of amyloid fibrils at a molecular level, e.g., the regions in a protein, say insulin, that form and stabilize the fibril core [2]. Yet, very little is known about the thermodynamics and nucleation mechanisms of aggregation leading to large scale fibrils and plaques, which is crucial to the pathogenesis of protein deposition diseases [1,2]. The origin of the amyloid deposits and their precursors remains, thus, elusive despite being very important for the rational design of successful therapeutic strategies. By molecular-dynamics simulations, here we derive the aggregation mechanisms and equilibrium phase diagram of a system of molecules interacting via the realistic potential, which was recently experimentally determined for insulin monomers [3].

A growing body of evidence suggests that formation of ordered aggregates, the so-called amyloids, is a common generic feature to a class of proteins [1,2]. Among these, insulin has become a model system due to its medical importance and the wealth of available data. Oligomerization and fibril formations of this protein have been, thus, investigated by several experimental methods, and we know that fibril assembly is preceded by formation of a wide range of aggregates such as unstructured oligomers and structured amyloid protofibrils (see, e.g., [4–6], and references in [2]). Computer models have been proposed to study the molecular origin of those processes (see review in [2]), for instance, to explain the structure acquired by fibrils and the role of polyglutamine repeats (see [7,8] and references therein), to predict protein sequences stabilizing amyloid fibrils (see [9,10] and references therein), and the nature of intermolecular forces defining the fibril material properties [11]. A statistical-mechanics "four-bead" protein model shed light on monomer folding and their aggregation into oligomers, in correspondence with experimental observations [12], and a sequence-independent mechanism has been discovered, by computer simulations, whereby polypeptide chains aggregate in metastable oligomeric states before converting into fibrils by thermodynamics mechanisms [13]. Within such a framework, recent experiments yielded new information on the intermolecular forces of the monomers in the preaggregated state of insulin solutions [3]. The system structure factor was experimentally determined at low concentrations and the "coarse-grained" monomer interaction potential $V(r)$ derived [3]: $V(r)$ is found to be in the class of the Derjaguin-Landau-Verwey-Overbeek (DLVO) potentials known to give rise to complex particle structures [14–19].

We investigate here, by computer simulations, a system composed of monomers interacting via such a realistic DLVO-type potential $V(r)$. Although information at the molecular level is inaccessible by such a coarse-grained description, its advantage with respect to previous models stems from the possibility to explore the collective properties of the system and derive its thermodynamics, phase diagram, and kinetics. The parameters responsible for the formation of aggregation seeds and the self-assembly of large scale structures are discussed. We show that fibrils and plaques arise as distinct stable thermodynamics phases reached by phase transitions from a low-concentration fluid phase of monomers or oligomers (see Fig. 1). Along with the equilibrium phases, different metastable long-living phases exist, including protofibril random percolating networks.

II. RESULTS

We consider a system made of N monomers of diameter σ, in a cubic box of linear size $L=18\sigma$, with periodic boundary conditions. Monomers interact via the following DLVO potential (see Fig. 2):

$$\frac{V(r)}{\epsilon} = \left(\frac{\sigma}{r}\right)^{36} - A\left(\frac{\sigma}{r}\right)^{6} + B\frac{\sigma}{r}e^{-\kappa(r/\sigma-1)}, \qquad (1)$$

where r is the monomer distance and ϵ is the energy scale; A, B, and κ are parameters to be fitted on real data. This poten-

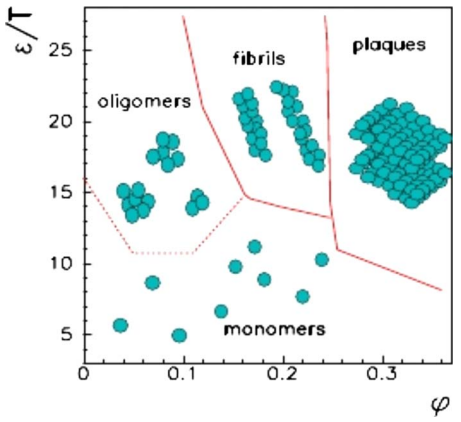

FIG. 1. (Color online) The system phase diagram comprises, at small volume fraction ϕ or interaction strength ϵ/T, a disordered phase of monomers or oligomers (schematically drawn). Those two regions are divided by a crossover (dotted line) marked by a change in the shape of the size distribution of the aggregates (see text). At higher ϕ, a phase transition occurs to a phase made of hexagonally packed long parallel fibrils. At even higher ϕ, a phase is found where plaques are formed.

tial is characterized by a hard-core repulsion, a short-range attraction, and a long-range repulsion. As discussed in Ref. [3], a DLVO interaction can fit the experimental structure factor $S(q)$ of insulin solutions. Indeed, Fig. 4 shows the data from Ref. [3] and a fit with the structure factor derived from Eq. (1): the experimental data of $S(q)$ refer to two distinct volume fractions with a 4 wt % and a 10 wt % solution of insulin at pH 2 [3]. Predictably, as already seen in [3], at high q (i.e., small length scales) a coarse-grained model produces a rough fit (solid lines in the inset of Fig. 4); however, the fit strongly improves in the region, we are interested in, of the peak at $\sigma q \sim 2$. The fitting parameters used here are $A=2.15$, $B=1.34$, $\kappa=2.04$, and $\epsilon/T=12.5$ (T is the temperature). They were determined by minimizing the squared deviation of $S(q)$ data sets and fit. The insulin diameter $\sigma=21$ Å is approximated from the material details given in Ref. [3].

Phase diagram. We discuss first the phase diagram of the system defined by the potential of Eq. (1) with the parameters determined above from experimental data, as a function

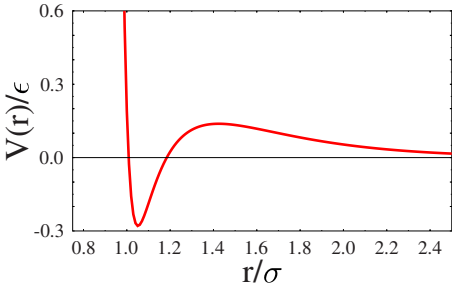

FIG. 2. (Color online) The DLVO interaction potential $V(r)$ used in this paper is plotted in units of the energy scale factor ϵ, as a function of the ratio of the monomer distance r and their diameter σ. $V(r)$ has a hard-core-like part, a short-range attraction, and a longer-range repulsion.

of two major control parameters: the volume fraction $\phi=\pi\sigma^3 N/6L^3$ and the ratio of the potential amplitude ϵ to the temperature T. Thermodynamically stable phases correspond to minima of the system free energy $\mathcal{F}$, which we computed by thermodynamic integration. To derive $\mathcal{F}$ for the disordered phase, the integration starts from the ideal-gas limit of randomly displaced monomers (high T, low ϕ); analogously, to derive $\mathcal{F}$ in the ordered phases, it starts from perfectly periodically arranged monomer structures in the form of fibrils or plaques. The stable phase at a given point $(\phi, \epsilon/T)$ in the space of the control parameters is the one having the smallest $\mathcal{F}$.

The resulting phase diagram is shown in Fig. 1. In the low ϕ and ϵ/T region, a disordered phase is found. Here, when the interaction energy ϵ/T is small enough, the system state is formed by independent monomers. At higher ϵ/T, a different region is observed where monomers aggregate into oligomers. We identify the monomers/oligomers crossover line (dotted line in Fig. 1) by the points, where the cluster size distribution $n(s)$ develops a peak corresponding to aggregates larger than a couple of units (see below), which becomes heavier than 50% of the total weight of the distribution. Oligomers are nearly spherical aggregates with a typical size of about 5–10 particles (see below). Interestingly, this is in close correspondence with known oligomerization properties of insulin [4,5] and in agreement with results from "four-beads" protein models [12]. From the oligomer phase, by increasing ϕ, the system transits into a new stable thermodynamic state corresponding to a fibrillar hexagonal columnar phase, where monomers are arranged in Bernal spirals. At even higher ϕ, a transition to a lamellar phase is observed, where plaques composed of two layers of particles (or more at higher ϕ) are formed. Size effects can change the precise boundary of the phases [20]. We tested that our considered sizes (volume and number of particles) are large enough to make them negligible.

In the monomer region, the particle cluster size distribution $n(s)$ is a monotonically decreasing function of s: by increasing s, $n(s)$ rapidly goes to zero and very few clusters larger than three or four particles are found at small volume fractions. At higher ϕ, the mean cluster size starts growing (see below) and seems to diverge at the percolation threshold located around $\phi \sim 0.15$ (the percolation threshold weakly depends on the ϵ/T value).

In the oligomer phase, $n(s)$ has a markedly different behavior (see Fig. 3): while a marginal peak at $s=1$ may still be observed, a new peak develops at higher values of s. It shifts in the range $s \simeq 5-10$ (and grows in height) as ϕ is increased. Correspondingly, as the percolation transition is approached from below, a long tail appears in the cluster size distribution ϵ/T. The typical values of $n(s)$ agree well with those reported in insulin experiments (see, e.g., [4,5]) and similar distributions are found β amiloyd with the four-beads model [12].

As shown in the inset of Fig. 3, the oligomer mean cluster size χ goes to a finite constant $\chi \simeq 5$ for $\phi \to 0$ and strongly grows when ϕ increases. It can be fitted by a power law diverging at the percolation point ϕ_p: $\chi \propto (\phi_p - \phi)^{-\gamma}$, with $\phi_p \sim 0.15$ and $\gamma \sim 1.4$.

The structure factor $S(q)$ (see Fig. 4) in the monomer region has two main peaks of approximately equal height

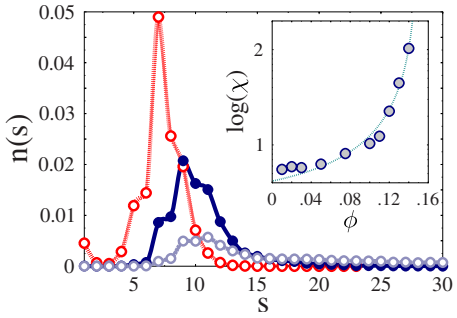

FIG. 3. (Color online) The oligomer size distribution $n(s)$ is plotted as a function of s, for three values of the volume fraction $\phi=0.05,0.10,0.13$ (from highest to lowest peak), and $\epsilon/T=23.7$. The inset shows the corresponding mean cluster size $\chi(\phi)$, i.e., the typical oligomer size, as a function of ϕ. The continuous line is a power-law fit $|\phi-\phi_p|^{-\gamma}$ defining the percolation point $\phi_p \simeq 0.15$ (and an exponent $\gamma \simeq 1.4$).

located around $\sigma q \simeq 2$ and $\sigma q \simeq 7.5$. The first is related to the long-range repulsive part of the potential $V(r)$; the second to the typical distance between nearest-neighbor particles set by the short-range attraction. In agreement with experimental results (see [3] and inset in Fig. 4), by increasing ϕ the first peak position remains approximately fixed while its height increases. In the oligomer region, two peaks are still present and located around similar q values. However, since here clusters on the order of ten particles are formed, the peak at $\sigma q \simeq 2$ grows on one order of magnitude.

The disordered oligomer region becomes metastable at high ϕ. Here, close to the percolation point, the first peak in $S(q)$ grows even further. Finally, in the ordered phases, it jumps to values on the order of the total number of particles in the system. Figure 5 shows the dynamics of the maximum $S_{\max}$ of $S(q)$ (at $\sigma q \simeq 2$) in the fibril phase: the system is initially prepared in a disordered configuration, having a

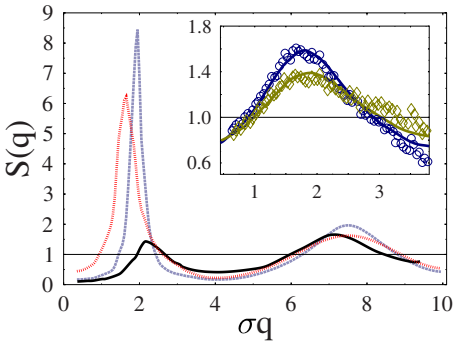

FIG. 4. (Color online) The shape of the structure factor $S(q)$ is shown in the monomer phase ($\epsilon/T=7.12$, $\phi=0.2$, black curve) and in the oligomer phase ($\epsilon/T=23.7$, and $\phi=0.05,0.13$, respectively, dotted red and dashed blue curves). The first peak of $S(q)$ is located close to $\sigma q \sim 2$, but its ϕ-dependent height is much higher in the oligomer than the monomer region. The inset shows the insulin experimental data of Ref. [3] corresponding to volume fractions of 4 wt % and 10 wt % (green diamonds and blue circles). As found in [3], a DLVO potential can fit the data: the continuous curves are the structure factors derived from simulations of a system of monomers interacting via the potential $V(r)$ of Eq. (1) (see text).

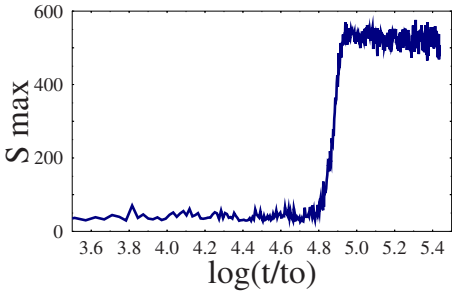

FIG. 5. (Color online) The typical dynamics of structure factor peak $S_{\max}$ (at $\sigma q \simeq 2$) is shown as a function of time t/t_0 for a system evolving toward the fibril phase ($\epsilon/T=17.8$, $\phi=0.15$), which is initially prepared in a monomer disordered state. After a nucleation time of approximately $10^5 t_0$, $S_{\max}$ has an abrupt change signaling the formation of fibrils.

small $S_{\max}$; it then evolves and, when fibril nucleation starts, $S_{\max}$ jumps abruptly to much higher values.

Dynamics. To investigate the system dynamics, as in the above example, and corroborate the picture emerging from the free-energy study, we simulated the system via molecular-dynamics simulations in the *NVT* ensemble by a Nosé-Hoover thermostat [21]. We prepare the system at the desired volume fraction ϕ with a very small interaction strength $\epsilon/T=1$, so that particles are approximately independent (apart from the hard-core repulsion). After the system has thermalized in such conditions, time is set to zero, the interaction ϵ/T to the desired value, and the kinetics recorded (the unit of time is $t_0=\sqrt{m\sigma^2/\epsilon}$).

When ϕ and ϵ/T are small, the system approaches its equilibrium state within comparatively short time scales. As anticipated by the analysis of $\mathcal{F}$, at small enough values of ϵ/T, a disordered phase of monomers is found. For ϵ/T above the range 10–14, oligomers are formed and at higher volume fractions, above $\phi \simeq 0.13$, clusters tend to coalesce into locally fibril-like quasi-one-dimensional structures, until at some point around $\phi \sim 0.15$ these structures percolate. The resulting network shares very similar features to those experimentally revealed [22]: it is composed by locally fibril-like segments, joined by branching points, and is highly disordered. This structure is, however, metastable and, at a time around $10^5-10^6 t_0$ (see Fig. 5), it spontaneously orders in a hexagonal packing of parallel long fibrils. Monomers along the fibril rearrange to form spiral structures, as a result of the optimization of competing interaction terms in the DLVO potential.

The time needed to form ordered fibrils depends strongly on the value of the control parameters. In the region where a percolating network appears, as discussed above (see Fig. 5), fibrils form afterward, in a time of about $10^5-10^6 t_0$; on the other hand, away from the percolation line, the nucleation time is much higher, above $10^7 t_0$. For such a reason, in molecular-dynamics simulations, plaque formation is more quickly observed when starting from a partially ordered initial state. Conversely, in the region where monomers are found at equilibrium, starting from an initial configuration made of plaques produces plaque "evaporation." Plaques remain, instead, stable in their corresponding region of the phase diagram.

As in glassy colloidal phenomena, the state of the system is, thus, found to depend on the interplay between long-lived metastable and stable phases. By increasing ϕ or ϵ/T, the system is driven out of its disordered equilibrium phase into a glassy region where, on long time scales, protofibrilar disordered aggregations appear. The latter, in turn, will eventually form thermodynamically stable columnar fibrils or plaques.

III. DISCUSSION

Interestingly, phenomena of aggregation into clusters, fibrils, and plaques share universal features across the vast class of amyloid proteins [1,2]. In the model case of insulin, recent experiments [3] revealed that monomers interact, at a coarse-grained level, via a potential in the DLVO class.

The full regime of validity of such a potential is still to be experimentally established, as much as its dependence on the specific experimental conditions [3]. Yet, while a number of complications may arise in practice, the determination of the monomer interaction potential opens the way to a full theoretical investigation of the model system (within its regime of validity) by statistical-mechanics methods.

Here, we investigated a realistic molecular system interacting by such a potential via two independent procedures: by finding the free-energy minimum via thermodynamic integration (to study equilibrium) and via molecular-dynamics simulations (to study dynamics/equilibrium). We derived a comprehensive scenario of its kinetics and thermodynamics, which reproduces the data from Ref. [3] and all the key experimental features of insulin monomer self-assembly. We showed that DLVO monomers are indeed prone to aggregation into oligomers and, by phase transitions, into fibrils and plaques, as summarized by the system equilibrium phase diagram. The kinetics of aggregation is very important as well, since long-lived metastable phases, such as protofibrillar networks, are encountered when volume fractions or interaction amplitudes are increased. Our phase diagram elucidates the role of two major parameters controlling the formation of fibrils/plaques, i.e., volume fraction and interaction strength of monomers.

As usually found in phase-transition phenomena, the precise locations of the boundaries between phases, and their details in general, depend on the specific values of the parameters in $V(r)$ (e.g., scale of long-range repulsion). Thus, they will be usually different for different protein systems. On the other hand, the physics of colloidal suspensions has revealed that the general topology of the phase diagram is not dependent on the details of DLVO. In this sense, a form of universality emerges, which could explain the deep similarity of aggregation processes in the vast class of amyloid materials.

[1] M. S. Forman, J. Q. Trojanowski, and V. M. Y. Lee, Nat. Med. **10**, 1055 (2004).
[2] F. Chiti and C. M. Dobson, Annu. Rev. Biochem. **75**, 333 (2006).
[3] N. Javid, K. Vogtt, C. Krywka, M. Tolan, and R. Winter, Phys. Rev. Lett. **99**, 028101 (2007).
[4] E. J. Nettleton *et al.*, Biophys. J. **79**, 1053 (2000).
[5] G. Bitan *et al.*, Proc. Natl. Acad. Sci. U.S.A. **100**, 330 (2003).
[6] T. P. J. Knowles *et al.*, Proc. Natl. Acad. Sci. U.S.A. **104**, 10016 (2007).
[7] M. Stork, A. Giese, H. A. Kretzschmar, and P. Tavan, Biophys. J. **88**, 2442 (2005).
[8] S. D. Khare, F. Ding, K. N. Gwanmesia, and N. V. Dokholyan, PLOS Comput. Biol. **1**, e30 (2005).
[9] A. M. Fernandez-Escamilla, F. Rousseau, J. Schymkowitz, and L. Serrano, Nat. Biotechnol. **22**, 1302 (2004).
[10] A. Trovato, F. Chiti, A. Maritan, and F. Seno, PLOS Comput. Biol. **2**, e170 (2006).
[11] T. P. Knowles *et al.*, Science **318**, 1900 (2007).
[12] B. Urbanc, L. Cruz, S. Yun, S. V. Buldyrev, G. Bitan, D. B. Teplow, and H. E. Stanley, Proc. Natl. Acad. Sci. U.S.A. **101**, 17345 (2004).
[13] S. Auer, F. Meersman, C. M. Dobson, and M. Vendruscolo, PLOS Comput. Biol. **4**, e1000222 (2008).
[14] R. P. Sear, S. W. Chung, G. Markovich, W. M. Gelbart, and J. R. Heath, Phys. Rev. E **59**, R6255 (1999).
[15] C. B. Muratov, Phys. Rev. E **66**, 066108 (2002).
[16] S. Mossa, F. Sciortino, P. Tartaglia, and E. Zaccarelli, Langmuir **20**, 10756 (2004).
[17] A. Imperio and L. Reatto, J. Phys.: Condens. Matter **16**, S3769 (2004).
[18] A. de Candia *et al.*, Physica A **358**, 239 (2005).
[19] A. de Candia, E. Del Gado, A. Fierro, N. Sator, M. Tarzia, and A. Coniglio, Phys. Rev. E **74**, 010403(R) (2006).
[20] G. Singh, I. Brovchenko, A. Oleinikova, and R. Winter, Biophys. J. **95**, 3208 (2008).
[21] M. P. Allen and D. J. Tildsley, *Computer Simulation of Liquids* (Oxford Press, New York, 2000).
[22] J. L. Jimenez *et al.*, Proc. Natl. Acad. Sci. U.S.A. **99**, 9196 (2002).